# Fracture Toughness and Adhesion of Transparent Al:ZnO Films Deposited on Glass Substrates

Xiaolu Pang, Hongjian Ma, Kewei Gao, Huisheng Yang, Xiaolei Wu, and Alex A. Volinsky

Al-doped zinc oxide films (AZO) of different thicknesses were deposited by reactive magnetron sputtering on glass substrates. Fracture toughness and adhesion of transparent AZO films were measured by indentation in air and water. Fracture toughness of glass is about 0.63 MPa·m$^{1/2}$. Under the same normal load, radial crack length shortened with the increase of AZO film thickness. When indented under deionized water, cracks in both glass and AZO films got longer, signifying corresponding decrease in the fracture toughness.

## 1. Introduction

Transparent and conductive thin films based on zinc oxide (ZnO) have been recently investigated for electronic and optoelectronic device applications, including transparent electrodes, solar cells, heat reflecting windows and sensors (Ref 1-3). However, while most researchers focus on ZnO optoelectronic characteristics, mechanical characterization has not drawn equal attention. Since materials' mechanical properties are size-dependent, thin films may exhibit different mechanical behavior compared with their bulk counterparts. Besides optical and electrical properties, mechanical properties of ZnO are crucial for device design, in particular when reliability issues are concerned, including delamination, brittle fracture, and fatigue degradation of thin film structures.

Zinc oxide films belong to a family of transparent conducting oxide (TCO) films. Mechanical properties of TCO films govern patterning accuracy and durability in commercial applications, including liquid crystal and organic light emitting displays, and solar cells. Thin film mechanical properties have been measured by scratch (Ref 2) and pull-off tests (Ref 3), although it is challenging to evaluate thin film adhesion. Indium tin oxide thin films are widely used in practical TCO film applications. Here, we focus on Al-doped ZnO films (AZO) as an alternative TCO material (Ref 4-6), since the price of indium is dramatically increasing.

A number of techniques have been used for ZnO thin films fabrication, including chemical vapor deposition, sol-gel, spray pyrolysis, molecular beam epitaxy, pulsed laser deposition, vacuum arc deposition, and magnetron sputtering (Ref 6). In the present study, magnetron sputtering was used to deposit AZO thin films. The influence of processing parameters on structural, electrical, and optical properties was studied.

## 2. Experimental Details

Al-doped zinc oxide thin films were deposited on glass substrates by reactive magnetron sputtering from 3″ ZnO target (99.99% pure) and Al target (99.99% pure) in Ar plasma at $10^{-1}$ Pa pressure. Distance between the substrate and the target was 90 mm. Deposition was performed in Ar with 250 W ZnO and 40 W Al radio frequency (RF) power at room temperature. Argon flow rate was kept at 15 sccm. Glass substrates were thoroughly cleaned in acetone, ethanol, and deionized water for 10 min, respectively, in order to remove organic contaminants using ultrasonic bath (Ref 7). Substrates were dried before loading in the deposition chamber, where they were etched for 15 min in Ar plasma at 100 W RF power to further clean the surface (Ref 8). Target 10 min pre-sputtering with 200 W was performed to get rid of impurities on the target surface. Films of different thicknesses were deposited for 20, 40, 60, 80, and 100 min, respectively, and the thickness was measured with the surface profiler, as shown in Fig. 1.

Glass is a brittle material, which cracks when loaded to a certain stress level. In this experiment, different loads were applied to glass and AZO film samples with various thicknesses. In addition, the influence of water on crack propagation was also considered. Prior to loading, water was placed on the glass and AZO film surface to determine whether it has an effect on the crack growth. First a smaller load was applied, then water was added, and a larger load was applied. This procedure allowed comparing glass and AZO films fracture properties in water.

Nanoindentation is widely used to measure thin films mechanical properties. From the nanoindentation curves, both elastic modulus and hardness can be readily extracted (Ref 9-12). Indentation techniques have also been used to measure thin film adhesion and fracture toughness (Ref 13-18). When a sharp tip, such as Berkovich, Vickers, or a cube corner

**Xiaolu Pang, Hongjian Ma, Kewei Gao,** and **Huisheng Yang**, Department of Materials Physics and Chemistry, University of Science and Technology Beijing, Beijing 100083, China; **Xiaolei Wu**, State Key Laboratory of Nonlinear Mechanics, Chinese Academy of Sciences, Beijing 100080, China; and **Alex A. Volinsky**, Department of Mechanical Engineering, University of South Florida, Tampa, FL 33620. Contact e-mail: pangxl@mater.ustb.edu.cn.
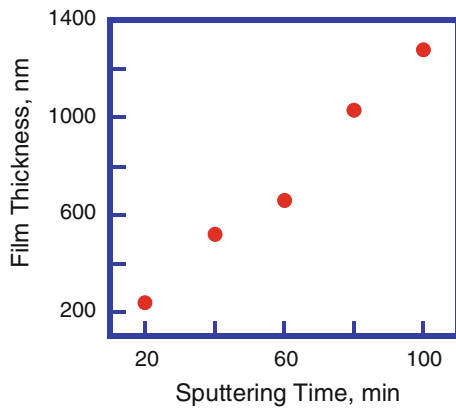
**Fig. 1** AZO film thickness as a function of sputtering time

diamond is indented into bulk brittle materials, radial cracks can occur at a critical load. Typically, the sharper cube corner diamond tip is used because of the greater stress concentration underneath the tip, which can induce fracture at lower critical normal loads. In the case of thin films, lower critical loads are necessary to minimize the inevitable substrate influence on the film fracture process. This method allows one to calculate fracture toughness based on the maximum indentation load and the crack length (Ref 19).

The analysis is complicated in the case of thin film radial fracture because of the half-penny crack shape perturbation by the substrate, film densification, and residual stresses in the film. However, current studies have yielded promising developments in this area. Vickers and nanoindentation residual impressions are shown in Fig. 2.

## 3. Results and Discussion

### 3.1 Transmittance of AZO Films

Films' transmittance was examined using U-3010 spectrophotometer (Hitachi, Japan). Transmitted spectra of AZO coatings with different thicknesses are shown in Fig. 3. Films become less transparent with the film thickness increase. A weak fluctuation in the spectrum is mainly due to optical interference between the film top and bottom surfaces with thicker coatings having more fluctuations (Ref 20). AZO films have a wider band gap than pure ZnO, thus it can be concluded that the short wave absorption limit of AZO films moves towards longer wavelength. As clearly seen in Fig. 3, UV absorption edge is shifted to the longer wavelength with increasing film thickness, indicating the broadening of the optical band gap. According to the quantum size effect theory, the smaller the grain size, the wider the energy gap is, along with the much longer displacement absorption edge. The number of carriers increases due to aluminum doping and the Fermi energy conduction band causing the energy band broadening (Burstein-Moss effect) (Ref 20).

### 3.2 Hardness and Elastic Modulus

Hardness, $H$, and elastic modulus, $E$, are two important thin film mechanical properties measured most frequently using nanoindentation techniques. Both elastic and plastic deformations occur, as the indenter is pressed into the sample, leaving a
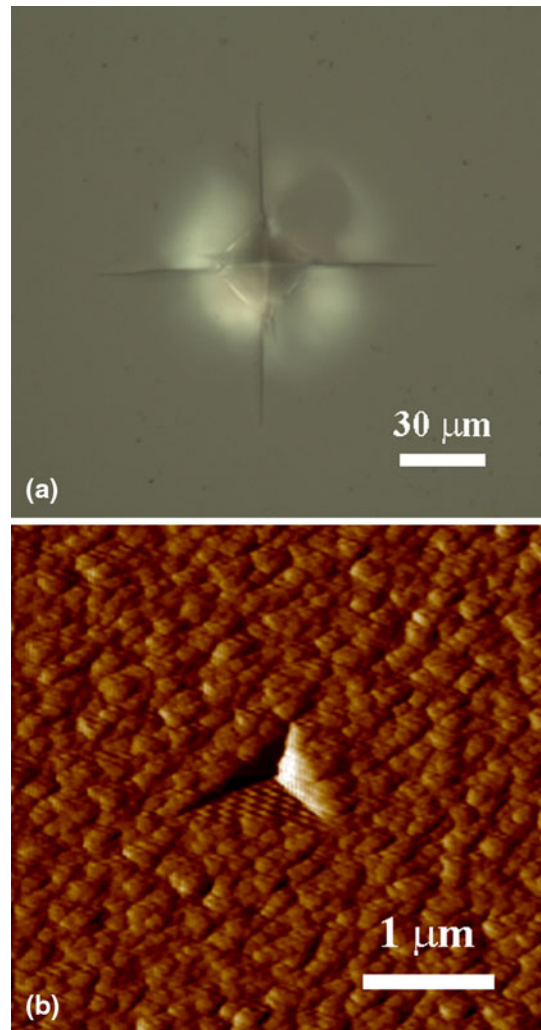


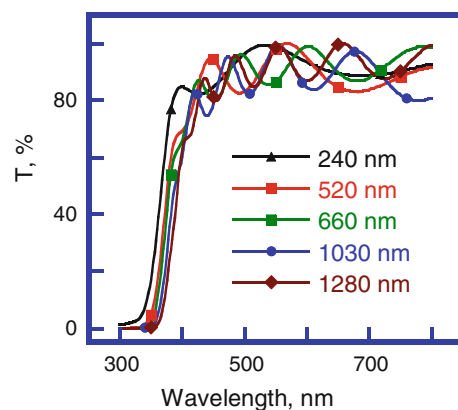**Fig. 2** (a) Vickers and (b) cube corner indentations



**Fig. 3** Transmittance of AZO films

permanent impression conforming to the indenter tip shape. During indenter withdrawal, only elastic portion of the displacement is recovered, which facilitates the use of an elastic solution in modeling the contact process (Ref 12, 21-23). Figure 4 shows a typical load-displacement curve, where $h_{max}$ represents the displacement at the peak load, $P_{max}$, and $h_c$ is the contact depth, defined as the depth of the indenter in contact
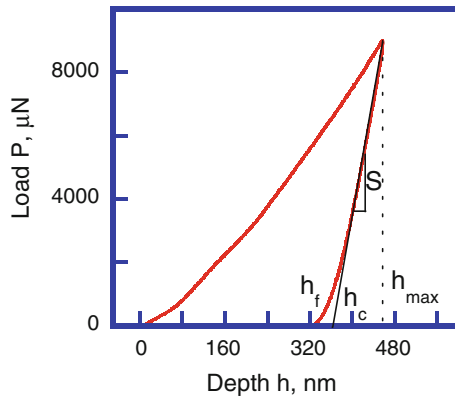
**Fig. 4** Load-displacement curve

with the sample under load, and $h_f$ is the final displacement after complete unloading. The slope of the load-displacement curve at the beginning of the unloading stage, $S$, is the indentation stiffness. Nanoindentation hardness is defined as the indentation load, $P$, divided by the projected contact area of the indenter, $A$:

$$H = \frac{P_{\max}}{A} \tag{Eq 1}$$

The elastic modulus can be determined from:

$$E_r = \frac{\sqrt{\pi}}{2} \frac{S}{\sqrt{A(h_c)}} \tag{Eq 2}$$

where $E_r$ is the reduced Young's modulus, and the sample elastic modulus, $E_s$, can be calculated from

$$\frac{1}{E_r} = \frac{\left(1 - v_s^2\right)}{E_s} + \frac{\left(1 - v_{tip}^2\right)}{E_{tip}} \tag{Eq 3}$$

Here, $v_s$ and $v_{tip}$ are Poisson's ratios of the sample and indenter tip materials, and, $E_{tip}$, is the elastic modulus of the tip.

### 3.3 Fracture Toughness of Glass With and Without Coatings

Table 1 shows radial crack lengths in glass and AZO films when indented by the Vickers' tip. In the experiments, each sample was indented with loads varying from 0.98 to 9.80 N. As expected, radial cracks in glass and AZO films are longer for higher loads. Radial cracks in glass are shown in Fig. 5. When indented with the same normal load, glass with AZO films had shorter cracks than bare glass. Furthermore, cracks became shorter with the film thickness increase. To account for this effect, fracture toughness, $K_{IC}$, is considered next. Fracture toughness is a mechanical property representing material's ability to resist crack propagation:

$$K_I = y\sigma(\pi a)^{1/2} \tag{Eq 4}$$

Here, $\sigma$ is the applied stress, $a$ is the crack length, and $y$ is a dimensionless constant related to the loading geometry. The radial tensile stress at the contact edge is given by Gerberich et al. (Ref 9):

$$\sigma = \frac{1 - 2v}{3} \left(\frac{6E^2P}{\pi^3 R^2}\right)^{1/3} \tag{Eq 5}$$

where $R$ is the radius of the indenter tip, which has been calibrated, $v$ is the Poisson's ratio, taken as 0.25 for AZO, and $P$ is the load.

Crack propagates when $K_I$ reaches the critical facture toughness value, $K_{IC}$. Fracture toughness of thin films can be measured by various methods, such as buckling, chipping, and indentation tests (Ref 8, 24). Indentation test is a popular method for thin film fracture toughness measurements (Ref 25).

Lawn and Marshall showed that a simple relationship exists between the fracture toughness, $K_{IC}$, and the length of the radial cracks, $c$ for bulk brittle materials (Ref 26):

$$K_{IC} = \alpha\left(\frac{E}{H}\right)^{1/2} \frac{P_{\max}}{c^{3/2}} \tag{Eq 6}$$

Here, $P_{\max}$ is the peak indentation load and $\alpha$ is an empirical constant, which depends on the indenter geometry. For well developed radial cracking produced by a Vickers indenter, the constant was found to be $0.016 \pm 0.004$ (Ref 27-29), while it is 0.039 for the Berkovich indenter and 0.032 for the cube corner indenter (Ref 30, 31). $H$ is the mean hardness, and $E$ is the elastic modulus, which can be determined using Eq 3 (Ref 32), where $E_{tip}$ and $v_{tip}$ represent the elastic modulus and the Poisson's ratio of the diamond indenter tip with the values of 1140 GPa and 0.07, respectively (Ref 26).

The simplicity of this technique makes it a common method to obtain fracture toughness of bulk brittle materials. However, the applicability of Eq 6 is somewhat restricted. Since fracture toughness is an intrinsic characteristic, the ratio of $P_{\max}/c^{3/2}$ should be constant. The linear relationship breaks down when $c/a_c \geq 2.5$, where $a_c$ is the contact radius of the impression (Vickers half-diagonal), discussed by Laugier (Ref 33), Nihara et al. (Ref 34), and Lima (Ref 35). However, Jang et al. (Ref 36) and Scholz et al. (Ref 37) found that such a scaling relationship was still valid even when the radial crack length was down to $1.1a_c$. Equation 6 was originally derived for bulk materials, as it assumes a half-penny shaped crack (Ref 38), and does not account for the elastic modulus mismatch between the film and the substrate.
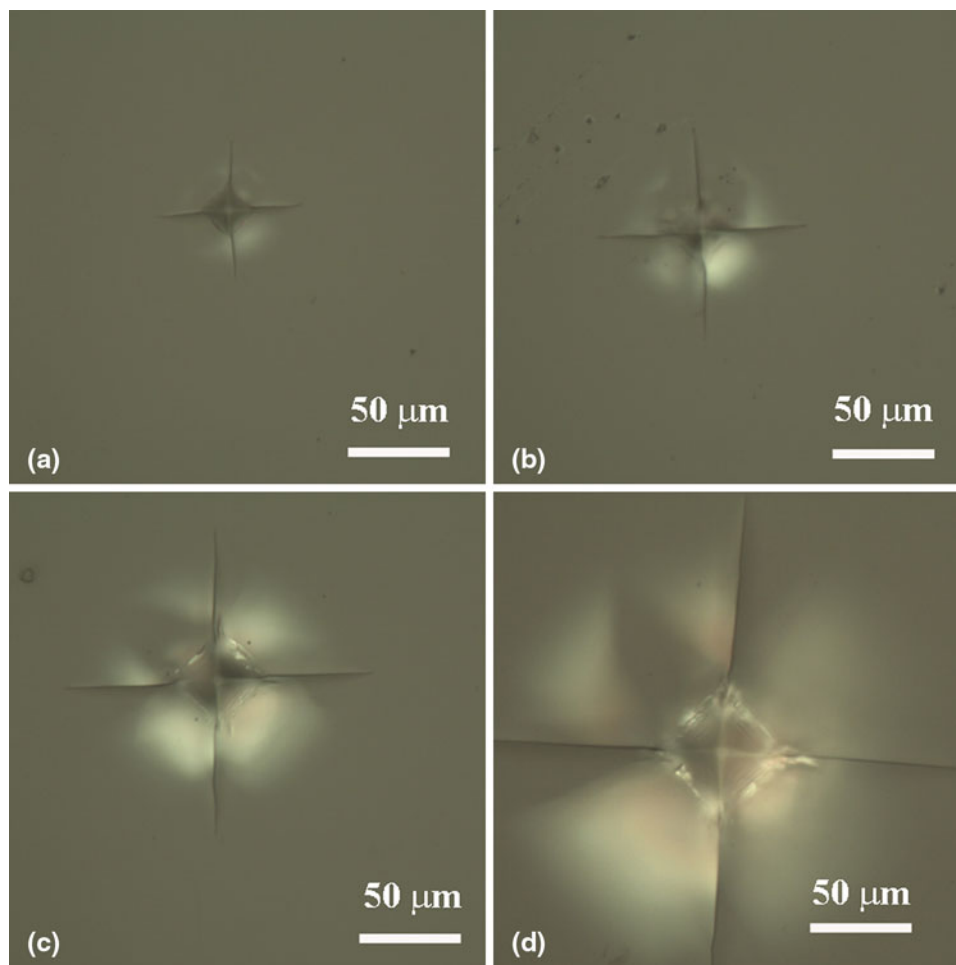
In case of glass in this experiment, it was indented by the Vickers tip, comparable with the above-mentioned requirements. For glass, cracks are half-penny shaped. The linear relationship of $P_{\max}$ and $c^{3/2}$ is obviously depicted in Fig. 6 for glass.

Nanoindentation technique is frequently used for obtaining the hardness and elastic modulus. The hardness, $H$, and elastic modulus, $E$, values for the coatings were obtained by extrapolating to zero depth determined by the Oliver and Pharr method at a range of maximum displacements (Ref 12). The $H/E$ ratios of some coatings and substrates from the literature are given in Table 2 (Ref 39).

The fracture toughness of glass as a function of the radial crack length is plotted in Fig. 7. The crack length measurement error is less than 5% and fracture toughness calculation error is no more than 20%. Thus it can be concluded that the fracture toughness of glass as a function of the radial crack length accounts for the intrinsic characteristic fracture toughness. The mean value of toughness obtained in this experiment is 0.63 MPa·m$^{1/2}$, which is in agreement with values quoted in the

**Table 1  Crack length in glass with and without AZO films**

| Sample | Load, N | | | | |
|---|---|---|---|---|---|
| | 0.98 | 1.96 | 2.94 | 4.90 | 9.80 |
| Glass | 10.32 μm | 28.65 μm | 39.88 μm | 59.60 μm | 98.90 μm |
| AZO: 240 nm | ... | 16.13 μm | 22.31 μm | 38.81 μm | 75.16 μm |
| AZO: 520 nm | ... | 14.81 μm | 21.74 μm | 36.44 μm | 73.24 μm |
| AZO: 660 nm | ... | 14.68 μm | 21.41 μm | 36.35 μm | 71.49 μm |
| AZO: 1030 nm | ... | 13.47 μm | 19.69 μm | 31.09 μm | 70.47 μm |
| AZO: 1280 nm | ... | 12.40 μm | 19.31 μm | 31.50 μm | 68.38 μm |



**Fig. 5**  Radial cracks in glass as a function of load: (a) 1 N, (b) 2N, (c) 3 N, and (d) 10 N

literature (0.62 MPa·m$^{1/2}$ for the float glass (Ref 40), and 0.71 MPa·m$^{1/2}$ for the soda lime glass (Ref 41)).

Compared with glass, it is more complicated to obtain the accurate values of AZO films fracture toughness. The hardness and the reduced Young's modulus of AZO film with a thickness of about 1030 nm are shown in Fig. 8. Equation 5 is valid only when $c/a_c \geq 2.5$, that is to say, $P_{max}/c^{3/2}$ ratio is an invariable constant. But for AZO films, which do not meet this requirement, the expression should not be directly applied in the case of a thin film, since typically the crack is no longer half-penny shape. It is not applicable for thin films on hard substrates, where the cannel crack is constrained and does not

kink into the substrate. The nonlinear relationship is also depicted in Fig. 6.

In this experiment, different thicknesses of AZO films of 240, 520, 660, 1030, and 1280 nm, were prepared by RF magnetron sputtering. They were indented by Vickers indenter tip with 0.98, 1.96, 2.94, 4.90, and 9.80 N normal loads. Opposite to glass, AZO films had no cracks under 0.98 N load, while glass had 10 μm cracks. Besides, with the increase of the film's thickness, the crack length continued to decrease. For AZO films of the same thickness, crack length increased with the load. As the load increased from 0.98 to 9.80 N, the crack length got longer, up to 73.2 μm. For AZO films under the
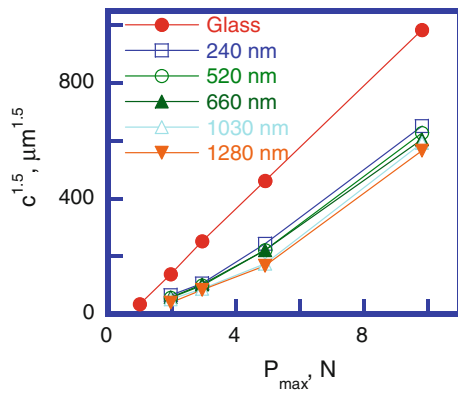
**Fig. 6** $c^{3/2}$ as a function of the maximum load

**Table 2** *H/E ratio of some coating and its glass substrate obtained by nanoindentation at the maximum loads from 100 μN to 1 mN load using a calibrated cube corner indenter (tip radius <100 nm) (Ref 39)*

|  | $E_r$, GPa | $H$, GPa | $E_r/H$ |
|---|---|---|---|
| Uncoated soda lime glass | 79 | 6.5 | 12.2 |
| ZnO coating | 114 | 15 | 7.6 |
| SnO2 coating | 131 | 14 | 9.4 |
| ITO coating | 133 | 12 | 11.1 |
| TiOxNy coating | 117 | 9 | 13.0 |



**Fig. 8** (a) Hardness and (b) reduced Young's modulus of AZO film with a thickness of 1032 nm
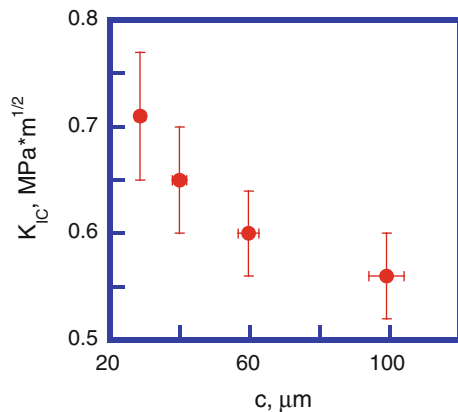


**Fig. 7** Glass fracture toughness as a function of radial crack length

same load, e.g., 9.80 N, the radial crack length decreased as the film became thicker. The results are listed in Table 1.

### 3.4 Water Effect

In real world applications, it is inevitable that AZO films will experience contact with water, thus studying water influence on film fracture under indentation is valuable. In brittle-coated systems, there are two types of fractures associated with indentation. Once fracture occurs, the properties of the film/substrate system will be affected. For instance, during a through-thickness fracture event in a brittle-coated system, the following changes in the mechanical response of the coated system may occur. The coating stiffness decreases. Plastic deformation of the substrate is more likely, or even dominates, while the elastic and plastic strains redistribute. The stored
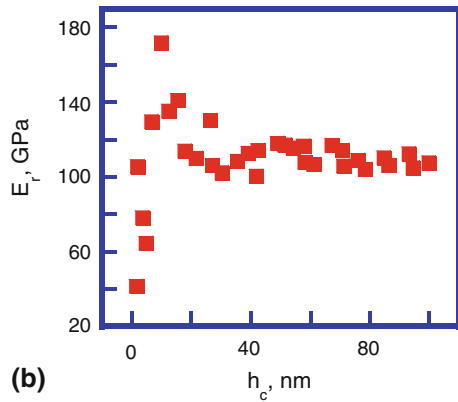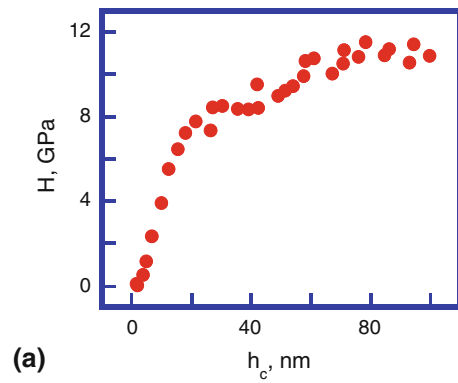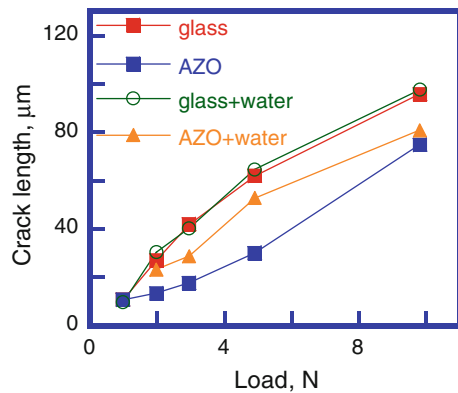


**Fig. 9** Cracks in glass and films indented in air and under water

elastic energy in the cracked coating is released; thus, during further deformation, this part of coating may be deformed elastically rather than plastically. Any membrane stress is released.

In this experiment deionized water was used for glass with and without AZO films of different thicknesses. Here, the results are shown in Fig. 9. In Fig. 9, lengths of cracks for glass and 1030 nm coating are plotted. The radial cracks are longer when both bare and coated glasses are indented under water. For bare glass, the change is not as obvious as for the coatings. This phenomenon was enhanced with increased load Table 3.

AZO films are under residual stress due to sputtering, thus this stress was released once indented under water. Vlassak and

**Table 3  Glass fracture toughness obtained using Eq 6**

| $P_{max}$ | $c$ | $P_{max}/c^{3/2}$ | $K_{IC}$, MPa·m$^{1/2}$ |
|---|---|---|---|
| 1.96 | 28.65±1.48 | 12.78 ±1.02 | 0.71±0.06 |
| 2.94 | 39.88 ± 1.99 | 11.67 ± 0.96 | 0.65 ± 0.05 |
| 4.90 | 59.60 ± 2.98 | 10.65 ± 0.85 | 0.60 ± 0.04 |
| 9.80 | 98.90 ± 4.95 | 9.96 ± 0.80 | 0.56 ± 0.04 |
| | | Avg: 11.27 ± 0.91 | Avg: 0.63 ± 0.05 |

co-workers (Ref 42, 43) pointed out that when films are exposed to water, the adhesion energy decreased as a result of water diffusion, but the crack velocity is limited due to diffusion of hydroxyl ions to the crack tip at high driving forces. Therefore, as seen in Fig. 9, when indented under water, more energy was released as the load increased for AZO films. At the same time, energy released rate decreased at higher load.

## 4. Conclusions

In this study AZO films were deposited by reactive magnetron sputtering on glass substrates. Fracture toughness and adhesion of transparent AZO films were measured by Vickers' indentation in air and water. The fracture toughness of glass is about 0.63 MPa·m$^{1/2}$ obtained using indentation, the radial crack length increased from 10.3 to 98.9 μm. For the AZO films, the crack length increased from 0 to 75 μm. Under the same load, radial crack length shortened with the increase of AZO films thickness. For either glass or AZO films of any thickness, the crack length increased as a function of indentation load. When indented in deionized water, cracks in both glass and AZO films were longer, which was especially obvious for the AZO films. Water diffusion decreases adhesion, and the crack extension velocity increases as a function of load.

## Acknowledgments

## References

1. X. Jiang, F.L. Wong, M.K. Fung, and S.T. Lee, Aluminum-Doped Zinc Oxide Films as Transparent Conductive Electrode for Organic Light-Emitting Devices, *Appl. Phys. Lett.*, 2003, **83**, p 1875

2. J. Yoo, J. Lee, S. Kim, K. Yoon, I.J. Park, S.K. Dhungel, B. Karunagaran, D. Mangalaraj, and J. Yi, The Properties of Surface Textured ZnO:Al Films for Thin Film Solar Cells, *Thin Solid Films*, 2005, **480**, p 213

3. M. Bender, E. Gagaoudakis, E. Douloufakis, E. Natsakou, N. Katsarakis, V. Cimalla, G. Kiriakidis, E. Fortunato, P. Nunes, A. Marques, and R. Martins, Production and Characterization of Zinc Oxide Thin Films for Room Temperature Ozone Sensing, *Thin Solid Films*, 2002, **418**, p 45

4. S. Kobayakawa, Y. Tanaka, and A. Ide-Ektessabi, Characteristics of Al Doped Zinc Oxide (ZAO) Thin Films Deposited by RF Magnetron Sputtering, *Nucl. Instrum. Methods B*, 2006, **249**, p 536

5. M. Suchea, S. Christoulakis, N. Katsarakis, T. Kitsopoulos, and G. Kiriakidis, Comparative Study of Zinc Oxide and Aluminum Doped Zinc Oxide Transparent Thin Films Grown by Direct Current Magnetron Sputtering, *Thin Solid Films*, 2007, **515**, p 6562

6. H. Zhou, D. Yi, Z. Yu, L. Xiao, and J. Li, Preparation of Aluminum Doped Zinc Oxide Films and the Study of Their Microstructure, Electrical and Optical Properties, *Thin Solid Films*, 2007, **515**, p 6909

7. W. Lin, R. Ma, W. Shao, and B. Liu, Structural, Electrical and Optical Properties of Gd Doped and Undoped ZnO:Al (ZAO) Thin Films Prepared by RF Magnetron Sputtering, *Appl. Surf. Sci.*, 2007, **253**, p 5180

8. X. Pang, K. Gao, F. Luo, Y. Emirov, A.A. Levin, and A.A. Volinsky, Investigation of Microstructure and Mechanical Properties of Multilayer Cr/Cr$_2$O$_3$ Coatings, *Thin Solid Films*, 2009, **517**, p 1923–1926

9. W.W. Gerberich, W. Yu, D. Kramer, A. Strojny, D. Bahr, E. Lilleodden, and J. Nelson, Elastic Loading and Elastoplastic Unloading from Nanometer Level Indentations for Modulus Determinations, *J. Mater. Res.*, 1998, **13**(2), p 421

10. M. Doerner and W.D. Nix, A Method for Interpreting the Data from Depth-Sensing Indentation Instruments, *J. Mater. Res.*, 1986, **1**, p 601

11. G.M. Pharr, W.C. Oliver, and F. Brotzen, On the Generality of the Relationship Among Contact Stiffness, Contact Area and Elastic Modulus During Indentation, *J. Mater. Res.*, 1992, **7**(3), p 613

12. W.C. Oliver and G.M. Pharr, An Improved Technique for Determining Hardness and Elastic Modulus Using Load and Displacement Sensing Indentation Experiment, *J. Mater. Res.*, 1992, **7**, p 1564

13. D.B. Marshall and A.G. Evans, Measurement of Adherence of Residually Stressed Thin Films by Indentation. I. Mechanics of Interface Delamination, *J. Appl. Phys.*, 1984, **56**, p 2632

14. J.J. Vlassak, M.D. Drory, and W.D. Nix, Simple Technique for Measuring the Adhesion of Brittle Films to Ductile Substrates with Application to Diamond-Coated Titanium, *J. Mater. Res.*, 1997, **12**(7), p 1900

15. M.D. Kriese and W.W. Gerberich, Quantitative Adhesion Measures of Multilayer Films: Part I. Indentation Mechanics, *J. Mater. Res.*, 1999, **14**(7), p 3007

16. M.D. Kriese and W.W. Gerberich, Quantitative Adhesion Measures of Multilayer Films: Part II. Indentation of W/Cu, W/W, Cr/W, *J. Mater. Res.*, 1999, **14**(7), p 3019

17. A.A. Volinsky, N.I. Tymiak, M.D. Kriese, W.W. Gerberich, and J.W. Hutchinson, Quantitative Modeling and Measurement of Copper Thin Film Adhesion, *Mater. Res. Soc. Symp. Proc.*, 1999, **539**, p 277

18. A.A.Volinsky, N.R. Moody, W.W. Gerberich, Interfacial toughness measurements for thin films on substrates, Acta Mater. 50/3 (2002) 441

19. D.S. Harding, W.C. Oliver, and G.M. Pharr, Cracking During Nanoindentation and Its Use in the Measurement of Fracture Toughness, *Mater. Res. Soc. Symp. Proc.*, 1995, **356**, p 663

20. K.E. Lee, M. Wang, E.J. Kim, and S.H. Hahn, Structural, Electrical and Optical Properties of Sol-Gel AZO Thin Films, *Curr. Appl. Phys.*, 2009, **9**, p 685

21. B. Bhushan, *Handbook of Micro/Nanotribology*, 2nd ed., CRC Press, Boca Raton, 1999

22. G.M. Pharr, Measurement of Mechanical Properties by Ultra-low Load Indentation, *Mater. Sci. Eng., A*, 1998, **253**, p 151–159

23. D.F. Bahr, D.E. Kramer, and W.W. Gerberich, Non-linear Deformation Mechanisms During Nanoindentation, *Acta Mater.*, 1998, **46**, p 3605

24. J. Malzbender, G. de With, and J.M.J. den Toonder, Elastic Modulus, Hardness and Fracture Toughness of Hybrid Coatings on Glass, *Thin Solid Films*, 2000, **366**, p 149

25. A.A. Volinsky, J.B. Vella, and W.W. Gerberich, Fracture Toughness, Adhesion and Mechanical Properties of Low-K Dielectric Thin Films Measured by Nanoindentation, *Thin Solid Films*, 2003, **429**, p 202

26. X. Pang, K. Gao, H. Yang, L. Qiao, and A.A. Volinsky, Annealing Effects on Microstructure and Mechanical Properties of Chromium Oxide Coatings, *Thin Solid Films*, 2008, **516**, p 4685

27. B.R. Lawn and A.G. Evans, Elastic/Plastic Indentation Damage in Ceramics: The Median/Radial Crack System, *J. Am. Ceram. Soc.*, 1980, **63**, p 574

28. G.R. Anstis, P. Chantikul, B.R. Lawn, and D.B. Marshall, A critical Evaluation of Indentation Techniques for Measuring Fracture Toughness: I. Direct Crack Measurements, *J. Am. Ceram. Soc.*, 1981, **64**, p 536

29. J. Chen and S.J. Bull, Indentation Fracture and Toughness Assessment for Thin Optical Coatings on Glass, *J. Phys. D: Appl. Phys.*, 2007, **40**, p 5403

30. B. Bhushan and X.D. Li, Nanomechanical Characterization of Solid Surfaces and Thin Films, *Int. Mater. Rev.*, 2003, **48**, p 125

31. X.D. Li, D.F. Diao, and B. Bhushan, Fracture Mechanisms of Thin Amorphous Carbon Films in Nanoindentation, *Acta Mater.*, 1997, **45**, p 4453

32. K.L. Johnson, *Contact Mechanics*, Cambridge Press, Cambridge, 1985

33. M.T. Laugier, New Formula for Indentation Toughness in Ceramics, *J. Mater. Sci. Lett.*, 1987, **6**, p 898

34. K. Nihara, R. Morena, and D.P.H. Hasselman, Evaluation of $K_{\rm Ic}$ of Brittle Solids by the Indentation Method with Low Crack-to-Indent Ratios, *J. Mater. Sci. Lett.*, 1982, **1**, p 13

35. M.M. Lim, C. Godoy, P.J. Modenesi, J.C. Avelar-Batista, A. Davison, and A. Matthews, Coating Fracture Toughness Determined by Vickers Indentation: An Important Parameter in Cavitation Erosion Resistance of WC-Co Thermally Sprayed Coatings, *Surf. Coat. Technol.*, 2004, **177–178**, p 492

36. J. Jang, S. Wen, M.J. Lance, I.M. Anderson, and G.M. Pharr, Cracking and Phase Transformation in Silicon During Nanoindentation, *Mater. Res. Soc. Symp. Proc.*, 2004, **795**, p 313

37. T. Scholz, G.A. Schneider, J. Munoz-Saldana, and M.V. Swain, Fracture Toughness from Submicron Derived Indentation Cracks, *Appl. Phys. Lett.*, 2004, **84**, p 3056

38. J. Deva Reddy, A.A. Volinsky, C.L. Frewin, C. Locke, and S.E. Saddow, Mechanical Properties of Single and Polycrystalline SiC Thin Films, Mater. Res. Soc. Symp. Proc. Vol 1049, 2008

39. J. Chen and S.J. Bull, Indentation Fracture and Toughness Assessment for Thin Optical Coatings on Glass, *J. Phys. D: Appl. Phys.*, 2007, **40**, p 5405

40. J. Malzbender, G. de With, and J.M.J. den Toonder, Elastic Modulus, Indentation Pressure and Fracture Toughness of Hybrid Coatings on Glass, *Thin Solid Films*, 2000, **366**, p 145

41. P.D. Warren, Determining the Fracture Toughness of Brittle Materials by Hertzian Indentation, *J. Eur. Ceram. Soc.*, 1995, **15**, p 201

42. J.J. Vlassak, Y. Lin, and T.Y. Tsui, Fracture of Organosilicate Glass Thin Films: Environmental Effects, *Mater. Sci. Eng. A*, 2005, **391**, p 172

43. Y. Lin, T.Y. Tsui, and J.J. Vlassak, PECVD Low-Permittivity Organosilicate Glass Coatings: Adhesion, Fracture and Mechanical Properties, *Acta Mater.*, 2007, **55**, p 2463